Journal of Volcanology and Geothermal Research 382 (2019) 81–91

Contents lists available at ScienceDirect

Journal of Volcanology and Geothermal Research

journal homepage: www.elsevier.com/locate/jvolgeores

Globally detected volcanic lightning and umbrella dynamics during the 2014 eruption of Kelud, Indonesia

Kirstin A. Hargie [a], Alexa R. Van Eaton [b,*], Larry G. Mastin [b], Robert H. Holzworth [c], John W. Ewert [b], Michael Pavolonis [d]

[a] Portland State University, Department of Geology, Portland, OR, USA
[b] U.S. Geological Survey, Cascades Volcano Observatory, Vancouver, WA, USA
[c] University of Washington, Department of Earth and Space Sciences, Seattle, WA, USA
[d] National Oceanic and Atmospheric Administration, Madison, WI, USA

ARTICLE INFO

Article history:
Received 2 May 2017
Received in revised form 29 August 2018
Accepted 15 October 2018
Available online 18 October 2018

Keywords:
Volcanic lightning
Plume dynamics
Explosive volcanism
Volcanic ash
Electrification
Umbrella cloud

ABSTRACT

Volcanic lightning shows considerable promise as a monitoring and research tool to characterize explosive eruptions. Its key strengths are rapid and remote detection, because the radio signals produced by lightning can propagate thousands of km at the speed of light. Despite these tantalizing properties, the scientific work on volcanic lightning has only recently started gaining momentum. Much more is needed to understand what lightning reveals about the evolution of an eruption in near-real time. Here we examine the timing and energy release of lightning generated by the eruption of Kelud volcano in Indonesia on 13 February 2014, as detected by the World Wide Lightning Location Network (WWLLN). The eruption column reached at least 26 km above sea level, representing the highest plume since the advent of global lightning networks in the last decade. Therefore, it provides valuable constraints on the electrification of end-member, sustained Plinian columns. We investigate the lightning in context with satellite images, photographs, and other published studies. Results show that the earliest satellite-detected activity was a thermal anomaly at ~15:46 UTC, corresponding to a directed blast at the onset of eruption (and only a few lightning strokes). Following a brief pause, the eruption produced a sustained column and umbrella cloud that spread outward into the tropical stratosphere. Rates of umbrella expansion provide an average mass eruption rate (MER) in the range of 8×10^7–1×10^8 kg s^{-1}. A more nuanced picture emerges from the time-varying MERs (determined between each satellite pass), which show rapid intensification during the first hour of eruption, followed by constant MER for about an hour, and waning toward the end (after ~17:50 UTC). At this stage, decreasing flux into the umbrella cloud coincides with column instability and formation of pyroclastic density currents, as recorded by photos from the ground ~17:45 UTC. We infer that some of the erupted mass partitioned into ground-hugging currents, leading to a lower apparent MER. Interestingly, there is not a 1:1 correlation between lightning intensity and MER over the course of eruption. Stroke rates increase sharply within the first 30–40 min (during rapid intensification of the plume), and then drop below 2 strokes per min once the MER remains constant. This suggests that electrification was controlled by the *rate of increase* in MER—in other words, the acceleration of particles out of the vent. We also show that lightning stroke-rates and energies are greatest within 50 km of the vent, even when the ash cloud extends >200 km downwind, indicating that lightning was focused in the regions of highest particle concentration and turbulence. Overall, we conclude that abrupt changes in lightning rates are clearly linked to changes in eruption behavior, and that rapid detection could aid monitoring efforts to characterize eruption rates or styles.

1. Introduction

The eruption of Kelud volcano (East Java, Indonesia) began on the evening of 13 February 2014. It started with a directed blast, devastating an area of 6–12 km^2 and destroying monitoring instruments near the volcano (Caudron et al., 2015; Maeno et al., 2019). After a short pause, an eruption column rose into the tropical stratosphere and spread out as an umbrella cloud (Kristiansen et al., 2015). The Plinian phase was intense and short lived (<3 h), producing 0.2–0.3 km^3 of basaltic-andesite tephra (dense-rock equivalent), with significant impacts on aviation and local communities (Maeno et al., 2019). For example, an aircraft flew under the umbrella cloud some hours after the start of eruption, leading to minor engine damage. The encounter emphasized a need to improve both how we characterize and communicate hazards from high-intensity eruptions (Lechner et al., 2017).

* Corresponding author.
E-mail address: avaneaton@usgs.gov (A.R. Van Eaton).

https://doi.org/10.1016/j.jvolgeores.2018.10.016

In this regard, there are some notable aspects of the 2014 eruption. First, the early destruction of *in situ* monitoring stations on the volcano made it challenging to detect eruptive activity in near-real time. Remote-sensing methods such as infrasound and satellite became more important to track the eruption (Caudron et al., 2015). Second, the volcanic plume was captured in exceptional detail by satellite. For example, CALIPSO retrievals around 18:13 UTC on 13 February show that the top of the umbrella cloud was located at 18–19 km altitude and contained gravity waves, with an overshoot reaching at least 26 km above sea level (Kristiansen et al., 2015). Third, abundant lightning strokes (~491) were documented by the World Wide Lightning Location Network (WWLLN) and photographed by observers (Fig. 1). Data from this network have been previously used to examine eruption dynamics during the 2015 eruption of Calbuco volcano, Chile (Van Eaton et al., 2016). However, many questions still exist regarding how and when globally-detectable lightning occurs during eruptions, and its relationship to source parameters like mass eruption rate (MER). In particular, the energy of volcanic lightning detected by WWLLN has never been investigated, yet may provide clues about eruption behavior. There is substantial motivation to determine what lightning can tell us about processes influencing transport and dispersal of volcanic ash (Behnke et al., 2018; Smith et al., 2018).

Here we examine the timing and energy release of lightning generated by the Kelud eruption. Our findings are placed in context with the volcanic plume dynamics, inferred from analysis of satellite imagery and photographs, and from published studies (e.g., Nakashima et al., 2016; Maeno et al., 2019). The overall aim is to develop a coherent picture of how lightning stroke-rates and energetics relate to the eruption behavior through time.

2. Methods

2.1. Volcanic lightning detection and analysis

Lightning emits broadband electromagnetic radiation, including very low-frequency (VLF) radio waves that can propagate thousands of kilometers from source. Even volcanic thunder (traveling as sound waves) has been detected up to 60 km away (Haney et al., 2018). The World Wide Lightning Location Network or WWLLN (http://wwlln.net) operates in real time and locates lightning anywhere in the world (Fig. 1a). Its Volcanic Lightning Monitor provides publicly available lightning locations within 100 km of every volcano listed in the Smithsonian Global Volcanism Program database (Ewert et al., 2010). Two-dimensional locations (latitude and longitude) are determined using the time of arrival of the VLF radio wave packets generated by lightning strokes, detected by five or more of the 80+ receiving stations worldwide. The location algorithm is described in detail by Hutchins et al. (2012a, b). Timing precision is <10 μs and spatial accuracy is <5 km (Hutchins et al., 2012a). For this study we consider the timing, location, and energy of Kelud's ~491 volcanic lightning strokes. We identified volcanic lightning from background thunderstorms using two criteria in post-analysis: (1) occurring within the known time period

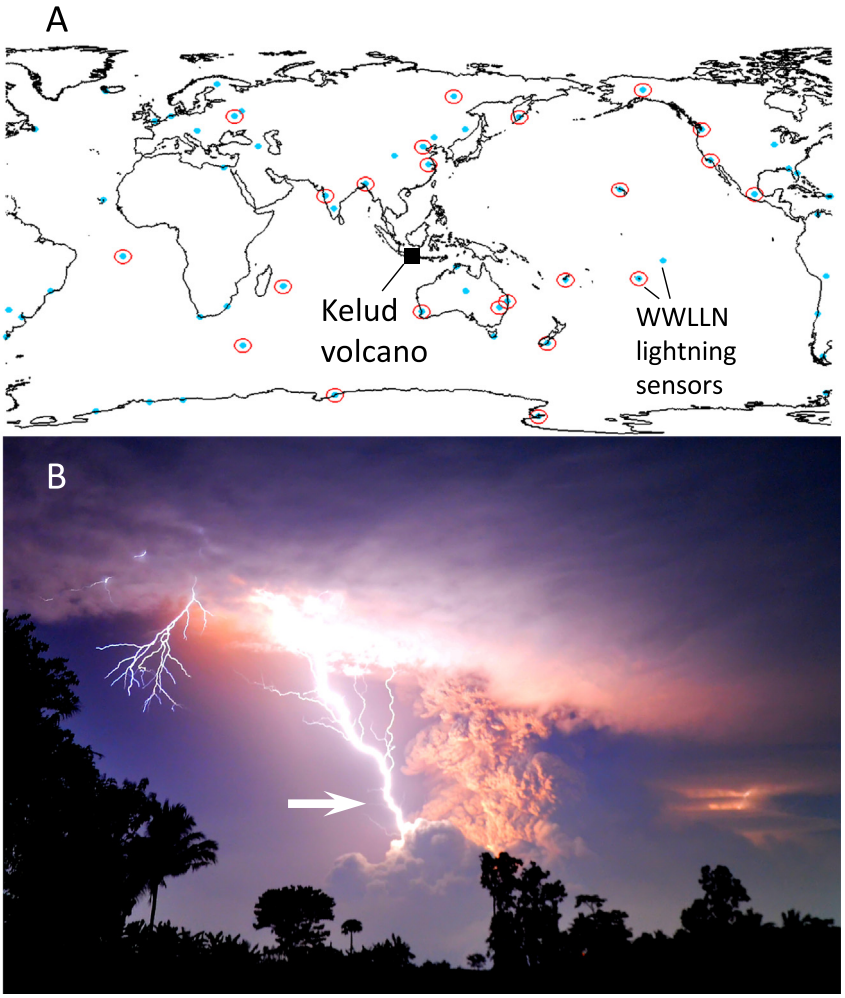

Fig. 1. Location map and example of lightning from the Kelud eruption on 13 February 2014. (a) Map showing Kelud volcano in East Java, Indonesia, and sensors of the World Wide Lightning Location Network (dots); circles show the sensors that detected lightning from this eruption. (b) Long-exposure photograph taken at 17:52 UTC from ~20 km south of the volcano, used with permission from Heppy Trisna Putra. Note volcanic lightning connecting the umbrella cloud and ground-hugging density current (arrow). Additional details and photos in Fig. 4.

of the eruption 15:30–20:00 UTC on 13 February 2014, and (2) spatially located within a bounding box from 76 km east, 200 km west, and 111 km north and south of Kelud volcano. All times are reported in UTC (local time is UTC +7 h).

It is worth mentioning some practical differences between the lightning detected by WWLLN and that which is visible to the naked eye, or other methods such as lightning mapping array (e.g., Behnke et al., 2013). WWLLN mainly sees the most energetic strokes. Studies of the network's relative detection efficiency indicate that it detects >50% of all strong lightning strokes (above 40 kA peak current), but only 10–30% of the weaker strokes (Hutchins et al., 2012b). Approximately two-thirds of detections are from cloud-to-ground lightning, with the remainder from intracloud or cloud-to-cloud discharges. The VLF energy of each return stroke is calculated from the far-field electromagnetic energy between 7 and 18 kHz, and is related to the peak current (Iwasaki, 2015).

2.2. Satellite and photograph analysis

The development of Kelud's airborne ash cloud was captured by MTSAT-2 and MTSAT-1R geostationary satellites, also known as Himawari-7 and -6, respectively (Figs. 2, 3). During the eruption, MTSAT-1R was in rapid scan mode, providing images at 10-minute intervals, with a few gaps (Fig. 3). All times reported for the satellite images used in this study give the scan time over Kelud volcano (with an uncertainty of ±20 s), rather than the start time of the image capture. For MTSAT-2 images, the difference is >10 min, but for MTSAT-1R, it ranges from 1 to 1.5 min. This is a small, but important revision of the detection times reported in previous studies. To determine the dimensions of the umbrella cloud through time, we used infrared brightness temperatures in the 11 μm channel. Two brightness temperatures were used to contour the outline of the umbrella. The −50 °C contour represents the center of the umbrella, including the overshooting top, which appears colder than the margins of the cloud due to its greater height, optical thickness, and degree of undercooling. The −30 °C contour represents the outer edge of the umbrella that is still visibly distinguishable from background. Both contours are used to help constrain the uncertainty of the analysis, using the method of Van Eaton et al. (2016). Brightness temperatures were contoured using Unidata's IDV software in the native satellite projection, and processed with ImageJ to calculate their areas at each time step. Where portions of the ash cloud merged with background atmospheric clouds, the outlines were manually interpolated using neighboring contours as a guide. Cloud areas were converted to radius of an area-equivalent circle (Supplementary Table 1).

A particularly valuable series of long-exposure photographs was taken from Blitar City, roughly 20 km south of Kelud Volcano (Fig. 4). These photos cover the time period from 17:38 to 18:00 UTC, showing spectacular features of volcanic lightning in the fully developed column and umbrella cloud.

3. Results and analysis

3.1. Satellite observations

Our interrogation of the satellite imagery indicates that the first sign of eruption was a thermal anomaly in the MTSAT-2 retrieval at 15:46:24 UTC (Fig. 2). Although the satellite began capturing the image at 15:32 UTC, it was actually >10 min later before the scan reached Kelud volcano. This is the earliest known start time of the eruption. Key features of the hot spot at 15:46 UTC include its: (1) abrupt appearance—the anomaly was not present in any other images in the 3.9 μm channel; (2) strong signal, ~21 K above background; and (3) large area, affecting a total pixel area of ~89 km^2, although the hot target may have been a sub-pixel feature (pixel size ~ 22 km^2). There is no corresponding anomaly in the MTSAT-1R imagery around this time, perhaps due to the larger viewing angle of that satellite and therefore, larger pixel size. The high-temperature anomaly may be related to a hot ballistic field ejected by the initial blast (rather than an ash cloud).

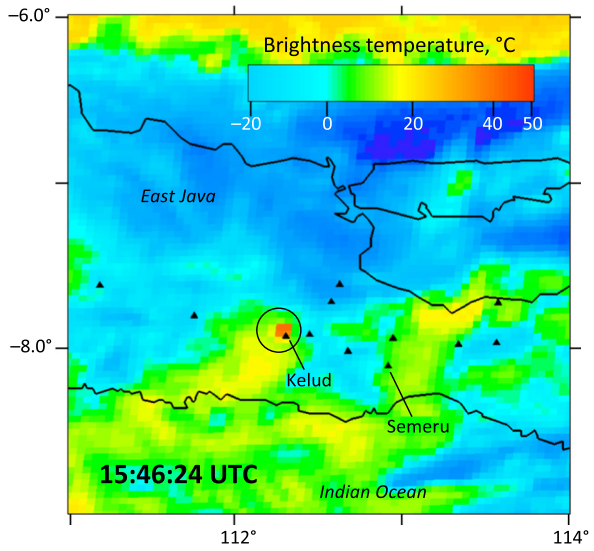

Fig. 2. Satellite image showing the earliest thermal anomaly detected during the 2014 eruption, at 15:46:24 UTC (hot pixels are circled). The thermal signature may have been caused by hot ballistic ejecta, rather than an ash cloud. Color scale gives MTSAT-2 brightness temperatures in the 3.9 μm channel. Black triangles show the active volcanoes in East Java, Indonesia, with Kelud and Semeru labeled for reference. Time stamp gives the time that the satellite scanned over Kelud volcano.

Fig. 3 shows the evolution of the airborne plume in MTSAT-1R, overlain with volcanic lightning locations detected by WWLLN. Note that the lightning plots are cumulative, adding to the previous detections for each time step. There is a very faint ash cloud as early as 16:10, which continues expanding radially as an umbrella cloud until reaching an upwind stagnation point from 17:00–18:10 UTC. After 18:10, the umbrella begins receding in the upwind direction, and finally detaches from the vent between 19:00–19:30. Dimensions of the umbrella cloud through time are shown in Fig. 3 and Supplementary Table 1. The umbrella growth series was used in two sets of calculations: (1) a time-averaged MER for the entire eruption, and (2) incremental MER from the growth rate between each individual satellite image, as described below.

3.2. Determining time-averaged MER

The expansion rate of an umbrella cloud provides an indication of the mass eruption rate feeding the plume (Sparks, 1986; Pouget et al., 2013). Growth of the umbrella radius (R), in meters, after time (t) in seconds since the start of eruption is proportional to the volumetric flow rate (V) of ash, gas, and entrained air injected into the umbrella region (in m^3 s^{-1}). Assuming that the umbrella expands outward as a gravity-driven intrusion, its growth rate is commonly assumed to be proportional to ~$t^{2/3}$ (Woods and Kienle, 1994),

$$R = \left(\frac{3\lambda N V}{2\pi}\right)^{1/3} t^{2/3} \quad (1)$$

where λ is an empirical cloud shape factor, taken as 0.2 after Suzuki and Koyaguchi (2009). N is the Brunt-Väisälä frequency of the atmosphere, calculated as 0.015 s^{-1} from radiosonde measurements at Surabaya Airport, using the method of Mastin (2014). Although most studies have previously assumed a ~$t^{2/3}$ relationship (Suzuki and Koyaguchi, 2009; Costa et al., 2013; Mastin et al., 2014), recent work by Pouget et al. (2016) and Suzuki and Iguchi 2019 suggested it may be more

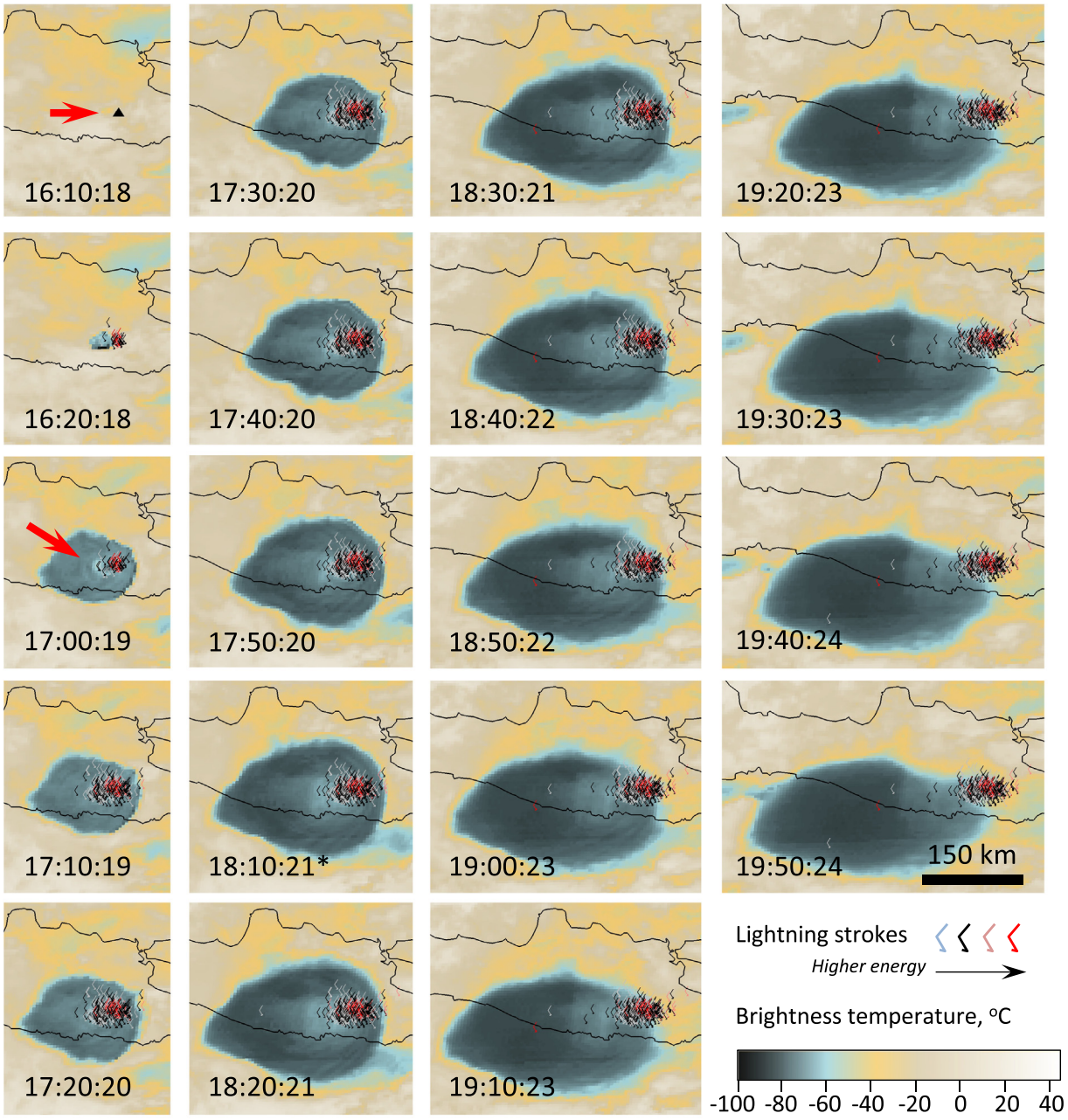

Fig. 3. Umbrella cloud development and lightning during the 13 February 2014 eruption of Kelud. Satellite images show MTSAT-1R Infrared brightness temperatures in the 11 μm channel, with the outline of the East Java coastline. Symbols show cumulative lightning strokes detected by WWLLN, with colors indicating relative stroke energy—red is more energetic. Times are in UTC, showing the scan time over Kelud (volcano shown as black triangle in first image). Note that parallax effects due to satellite viewing angle displace the plume a few km west of the volcano. Top arrow points to the faint initial plume. Lower red arrow points to gravity waves that appear in the 17:00 image. Gaps in satellite data occur between 16:20–17:00 and 17:50–18:10 UTC. (*) Indicates the image that roughly corresponds to the CALIPSO pass at 18:13 UTC (Kristiansen et al., 2015).

appropriate to assume a different power-law exponent, or one that changes during different stages of column development. In this case, we retained the ~$t^{2/3}$ relationship simply because it provided the best fit to the entire Kelud growth series (linear regression coefficient $r^2 > 0.99$ on a plot of $t^{2/3}$ vs. umbrella radius). We note that the governing equations are currently under revision by Webster et al. (in preparation).

Using these assumptions, the volumetric flow rate into the umbrella can be converted to a mass eruption rate M (in kg s^{-1}) according to Morton et al. (1956); Sparks (1986):

$$M = \left(\frac{VN^{5/8}}{Ck_e^{1/2}} \right)^{4/3}, \quad (2)$$

Fig. 4. Photographs of lightning during the Kelud eruption, taken from Blitar City, roughly 20 km south of the volcano. Exposure times are 30 s. In d–f, notice the left (western) margin of the eruption column: (d) shows a vertical, stable margin, then in (e) the margin becomes billowy, and in (f) pyroclastic density currents are visible near the ground. Photographs by Heppy Trishna Putra, used with permission.

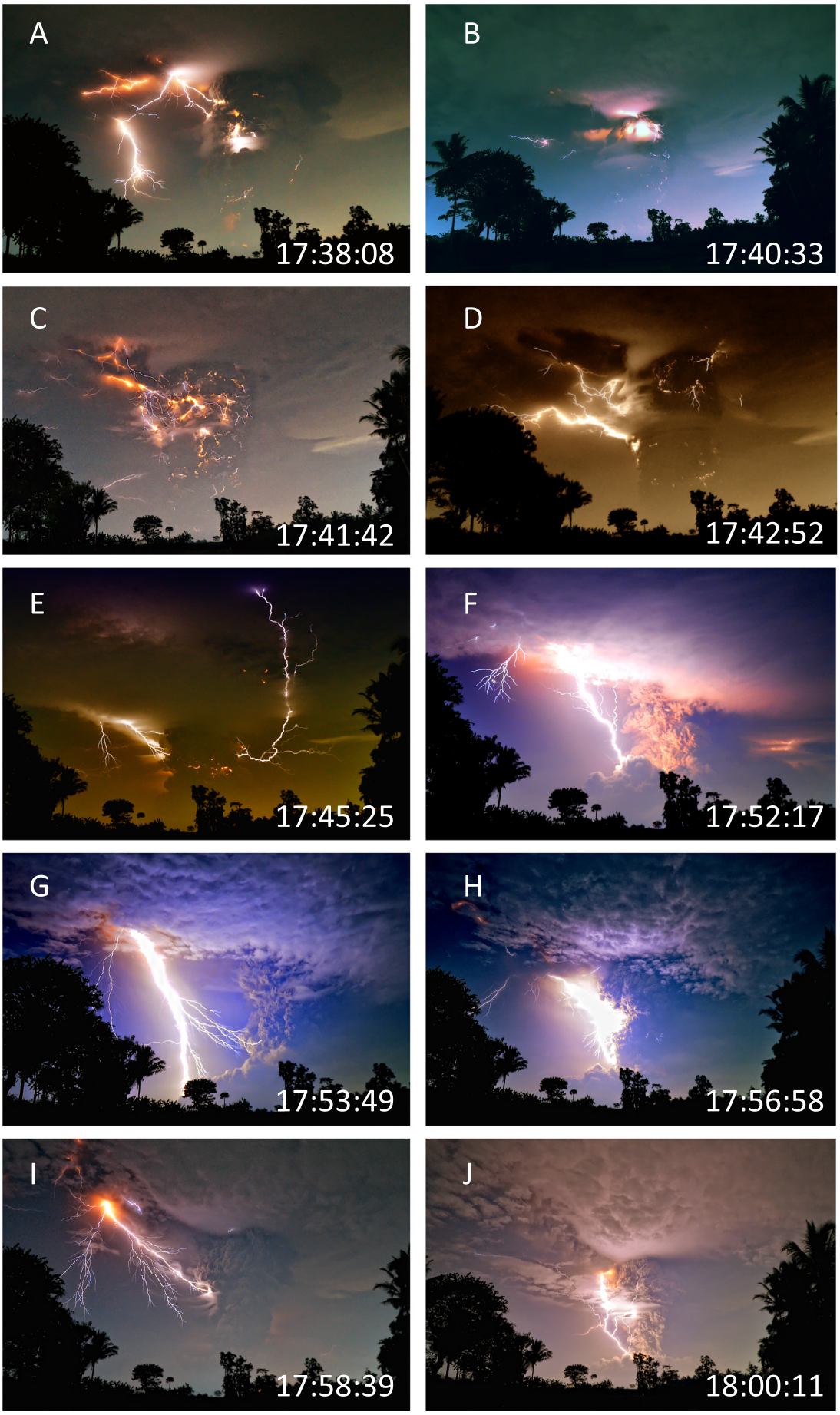
A
17:38:08
B
17:40:33
C
17:41:42
D
17:42:52
E
17:45:25
F
17:52:17
G
17:53:49
H
17:56:58
I
17:58:39
J
18:00:11

where k_e is the radial entrainment coefficient of the rising plume, taken as 0.1, and C is a proportionality constant, assumed to be 5000 $m^3\ kg^{-3/4}\ s^{-7/8}$ for tropical atmospheres (Suzuki and Koyaguchi, 2009; Mastin et al., 2014). Using Eqs. (1) and (2), the best-fit eruption start time and time-averaged MER were determined using a two-parameter best-fit function in Matlab. We applied this method to the satellite observations from 16:10–19:00 UTC, making the simplifying assumption that the MER stayed constant through the eruption. Back-calculating from the entire growth series using the −30 °C contour gives a start time of 16:09 UTC (Fig. 5). Other geophysical data indicate the Plinian phase actually began as early as 16:01 (Nakashima et al., 2016), but our analysis suggests that the eruption column did not begin to *intensify* until around 16:09. This timing is consistent with the first appearance of a faint ash plume in satellite imagery at 16:10 (Fig. 3). Best-fit curves through the two umbrella growth series (based on brightness temperatures of −50 and −30 °C) indicate a time-averaged MER between 8.3×10^7 and 1.3×10^8 kg s^{-1} (Fig. 5), providing a mean value of 1.1×10^8 kg $s^{-1} \pm 22\%$. Note that the warmer edge of the cloud expands more rapidly, giving a greater mass eruption rate. To provide a sense of the sensitivity of the results to variables used in Eq. (2), consider the value of C. Our calculations assumed a proportionality constant (C) for tropical atmospheres based on the modeling work of Suzuki and Koyaguchi (2009), but doubling this value to 10,000 $m^3\ kg^{-3/4}\ s^{-7/8}$ (more appropriate for the midlatitudes) decreases the best-fit MER by about 50% to ~6×10^7 kg s^{-1}. Therefore it is reasonable to expect an uncertainty of +/− 50% for the umbrella-derived MER using this approach.

3.3. Determining incremental MER

We also calculated the step-by-step MER using the umbrella growth rate between each satellite image. At a given time, if one can derive the eruption start time and establish values for λ and N, it is possible to calculate a volume flux V using a rearrangement of Eq. (1):

$$V = \left(\frac{2\pi}{3\lambda N}\right)\frac{R^3}{t^2}, \tag{3}$$

Using the cloud radii at two different times, two independent values were determined for V_1 and V_2. The average volume flux for a given time interval was then calculated using:

$$V_{avg} = \frac{V_1 + V_2}{2} = \left(\frac{\pi}{3\lambda N}\right)\left(\frac{R_1^3}{t_1^2} + \frac{R_2^3}{t_2^2}\right) \tag{4}$$

The resulting, average volume flux between each satellite image was converted to MER using Eq. (2), and assuming an onset time of 16:09 for intense development of the eruption column.

4. Discussion

4.1. Insights into eruption timing and plume dynamics

Fig. 5 summarizes the eruption timeline by plotting the umbrella cloud growth series (and time-averaged MER) along with lightning stroke-rates and energy. This figure only includes the lightning strokes within 20 km of Kelud volcano to focus on the proximal lightning most sensitive to changes at source. Three features are apparent: (1) intensification of the MER over the first hour of the eruption corresponds to the greatest lightning stroke rates; (2) roughly constant MER from 17:10–17:50 UTC corresponds to a drop in lightning rates; and (3) the MER steadily declines to the inferred end of eruption ~19:00 UTC (when the umbrella cloud begins detaching from the vent in satellite view, Fig. 3).

4.1.1. Directed blast

We infer that the hot spot detected in MTSAT-2 imagery at 15:46:24 UTC represents the earliest phase of eruption (Fig. 2). Studies of the volcanic deposits by Maeno et al. 2019 describe the opening phase as an explosion of Kelud's summit dome, resulting in a directed blast covering 6–12 km^2. An onset of ~15:46 UTC is consistent with other visual and geophysical observations. For example, ballistics were recorded in webcam images from the crater rim at ~15:45 UTC directly before the camera was destroyed (Maeno et al., 2019). And Nakashima et al. (2016) found that ground-coupled airwaves in the seismic record originated from Kelud volcano at ~15:46 UTC. Three lightning strokes were detected by WWLLN from 15:48–15:56 UTC, located <4 km of the volcano. We infer that lightning developed in the ground-hugging density current and lofted cloud, akin to the lateral blast from Mount St. Helens on May 18th, 1980 (Hoblitt, 2000), albeit much smaller (covering <12 km^2 compared to 600 km^2). Local photographs also capture this co-blast plume as a sluggish, slightly bent-over cloud rising into the lower atmosphere at 15:57 UTC (https://twitter.com/hilmi_dzi/status/434012442490703872/photo/1).

4.1.2. Plinian phase

Following ~15 min of relative quiet after the initial explosion, renewed activity was detected at 16:01:30 UTC as continuous acoustic tremor. Nakashima et al. (2016) interpret this as the start of the Plinian eruption, and the MTSAT-IR satellite retrievals show the first hint of an ash plume at 16:10 UTC (arrow in Fig. 3). We infer that the "apparent" onset time of 16:09 UTC (back-calculated from the umbrella growth series in Fig. 5) actually provides the intensification of the eruption rate after a sluggish onset some 8 min earlier. Volcanic lightning reappears at 16:12 UTC, after a ~15 min pause (Fig. 6). Lightning rates increase to >2 strokes per min until ~17:00 UTC (Fig. 6). The uptick in lightning corresponds to a rapid increase in MER determined by the incremental umbrella expansion method (Fig. 6). Interestingly, a solid-earth Rayleigh wave was produced at 16:14:30, which Nakashima et al. (2016) suggest may have been caused by dome destruction or vent erosion. This event occurs just a few minutes after our inferred start of eruption intensification, suggesting that vent widening may have accompanied the increase in MER (e.g., Fee et al., 2017). Reverse grading in the basal fall deposits (Maeno et al., 2019) further supports the concept of increasing MER in the initial Plinian phase.

Another intriguing observation by Nakashima et al. (2016) is that ground-coupled airwaves begin ~16:25 UTC, about 16 min after intensification of the Plinian column. These long period seismic signals (periods of 200–333 s) continued until ~19:00. We propose the ground-coupled airwaves were produced by gravity waves in the umbrella cloud once it began to spread in the stratosphere, as observed at Montserrat and Redoubt volcanoes (Ripepe et al., 2010; Lyons et al., 2013; Ripepe et al., 2016). In those cases, oscillations in the cloud generated atmospheric pressure waves that resonated in the solid earth. Indeed, gravity waves are visible in satellite views of the umbrella cloud by 17:00 UTC—appearing as concentric rings in the MTSAT-1R images (arrow in Fig. 3). They are still clearly visible more than an hour later during the CALIOP pass at 18:13 UTC (Fig. 2d,e of Kristiansen et al., 2015). Three-dimensional numerical simulations commonly reproduce these features as the rising column overshoots the level of neutral buoyancy and oscillates within a stratified atmosphere (Kanamori and Mori, 1992; Suzuki et al., 2016).

4.1.3. Shift in eruption style to column instability

From 17:00–18:10 UTC the umbrella maintained a constant upwind position, roughly 40 km east of vent. This stagnation point is thought to occur where the umbrella's expansion velocity equals the wind speed (Carey and Sparks, 1986). Nearby radiosonde profiles indicate wind speeds of 17 m s^{-1} at the umbrella height of 17–18 km asl. Between 18:10–18:20 UTC, the stagnation point began to recede downwind, suggesting a waning eruptive intensity, consistent with weaker remote seismoacoustic signals by 18:00 UTC (Caudron et al., 2015). Photographic

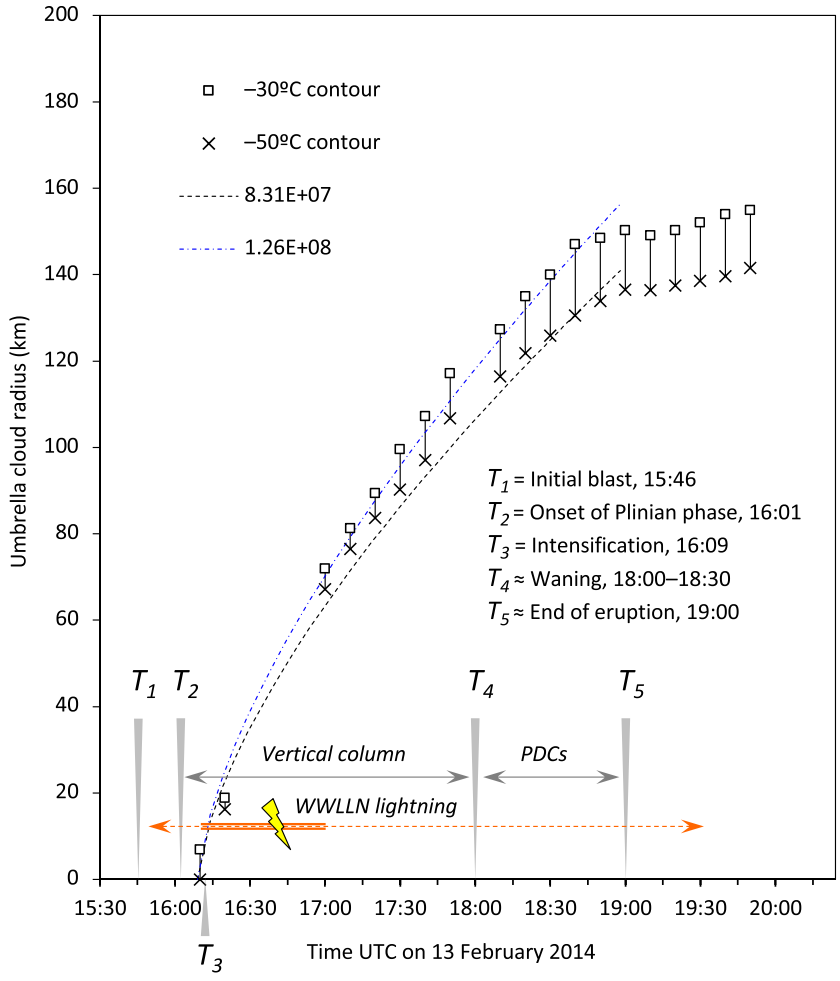

Fig. 5. Umbrella cloud expansion and time-averaged mass eruption rate. Equivalent radius of Kelud's umbrella cloud through time, defined by satellite infrared brightness temperatures of −30 and −50 °C. A two-parameter best fit through the entire growth series was calculated by adjusting the eruption onset time and MER, assuming a $t^{2/3}$ relationship. Theoretical growth rates are plotted showing the best-fit MERs, using an eruption start time of 16:09 UTC. Note differences in MER depending on how the umbrella outline is defined. Timing of eruption processes T1–T3 are from Nakashima et al. (2016) and modified by this study to include T4–T5. Eruption column behaviors—primarily vertical or PDC-generating—are from Maeno et al. 2019. Orange arrow denotes WWLLN-detected volcanic lightning, with bold line indicating lightning rates exceed 2 strokes per min.

and stratigraphic evidence also points to a significant change in eruption style, during which the vertical column began shedding pyroclastic density currents. There were a number of intraplinian flows before this point, but the transition after ~17:45 UTC is clearly visible in upper portions of the stratigraphy (S. Andreastuti, unpublished data). Photographs on the ground also show the shift to ground-hugging flows after 17:45 UTC (Fig. 4d–f). We suggest that the apparent decrease in MER after ~17:50 seen in the umbrella dynamics (Fig. 5) may be explained by some of the erupted mass feeding these ground-hugging currents rather than the high plume. A similar effect was observed during the 2015 eruption of Calbuco volcano in Chile (Van Eaton et al., 2016).

The eruption energy appears to ramp down after ~17:50. Lightning stroke-rates drop below 0.5–1 per min, and stroke energies remain $<10^4$ J (Fig. 6a,b). Nakashima et al. (2016) noted that resonant oscillations between the lower atmosphere and ionosphere (inferred gravity waves) ended around 18:45. And finally between 19:00–19:30 UTC, the umbrella separated from the vent in satellite (Fig. 3), indicating the end of significant ash emissions.

4.2. Relationship between lightning and eruption dynamics

There are some broad trends apparent in the lightning data from Kelud. Overall, lightning becomes lower-energy with distance from the volcano (Fig. 7). About 95% of the strokes are located within 50 km of Kelud in the downwind direction, and 30 km in the crosswind direction, even when the umbrella has expanded to >200 km diameter (Figs. 3, 7). The highest-energy strokes are also within 25 km of the vent (Fig. 7). These findings suggest that the production of globally-detectable lightning coincided broadly with the particle-rich, turbulent regions in the main updraft of the column and umbrella cloud. It is likely that this particle-rich, turbulent region hosted most of the lightning due to enhanced collision frequencies (triboelectric charging; Cimarelli et al., 2014; Méndez Harper and Dufek, 2016), combined with water condensation and freezing processes (ice charging; Deierling et al., 2008; Van Eaton et al., 2015, 2016).

Detailed examination reveals a subtler relationship between lightning and plume dynamics over time. Within the first ~50 min of the climactic eruption, during rapid intensification of the MER, lightning stroke-rates increase sharply (Fig. 6b). These strokes have lower median energy (Fig. 6a), with only a few high-energy outliers ($>10^4$–10^5 J), suggesting the eruption column was producing a lot of low-energy lightning. One possible explanation is that the eruption column was still well-mixed and turbulent during this vigorous phase, lacking sufficiently isolated 'layers' or 'pockets' of charge that would be needed to build up a huge electrical potential for powerful lightning. Instead, the well-mixed column produced numerous, smaller regions of charged particles within turbulent eddies, leading to numerous, smaller flashes (Behnke and Bruning, 2015; Behnke et al., 2013).

After this point, the MER stabilizes (remaining ~1×10^8 kg s^{-1} for about an hour), but lightning stroke-rates suddenly drop below 2 per

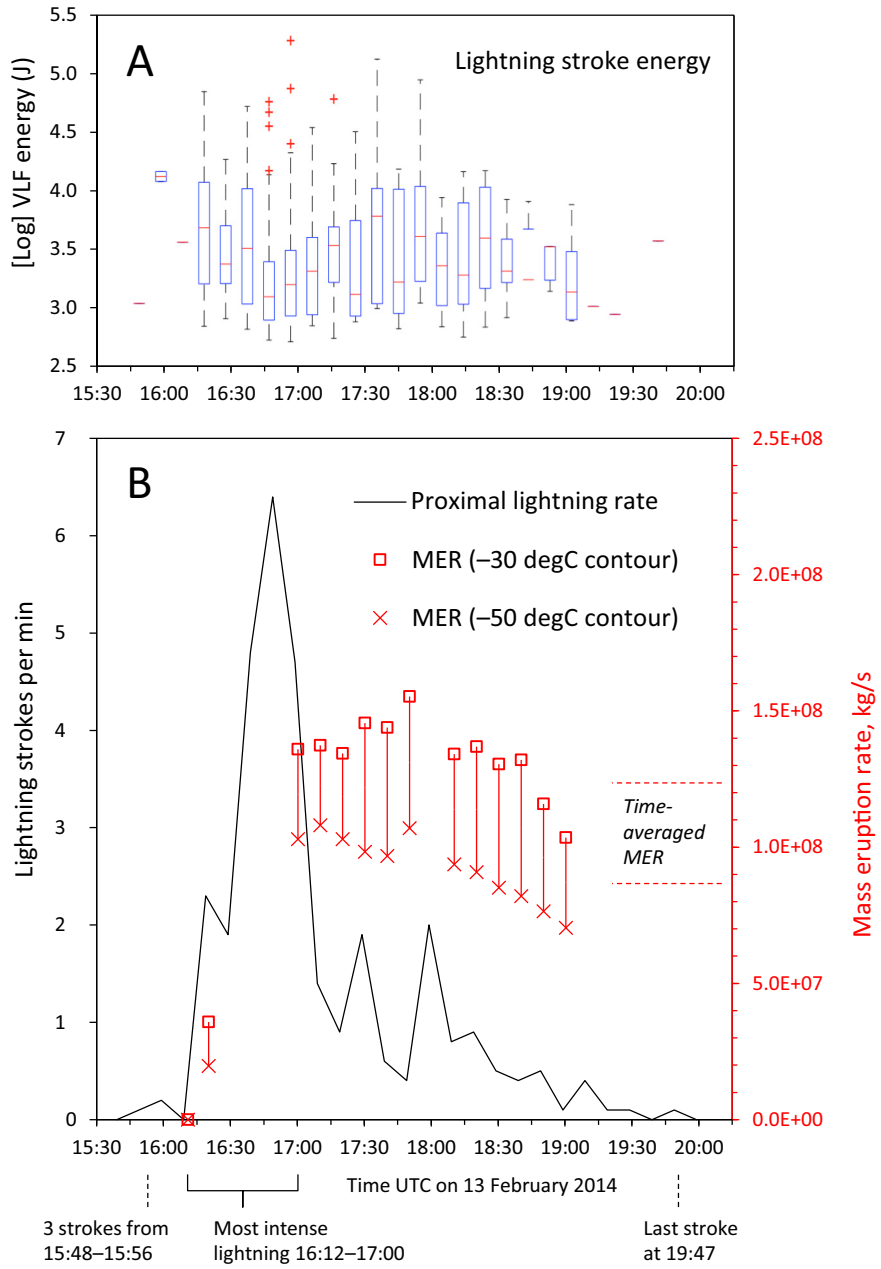

Fig. 6. Lightning stroke energy, stroke rate and mass eruption rate of ash emissions during the Kelud eruption on 13 February 2014. (A) Box and whisker plot shows stroke energy in the 7–18 kHz band, binned in 10-minute intervals. Note log10 scale on the y-axis. Boxes show the 25th and 75th percentiles, respectively. Whiskers show maximum and minimum values, defined by ±2.7σ. Red crosses are outliers; red lines show median values. Time intervals containing only one stroke are indicated with a single red line. (B) Rates of proximal lightning strokes in 10-minute intervals (note: these are only strokes within 20 km of Kelud). Right axis shows mass eruption rates determined by umbrella growth rates between each MTSAT-1R satellite pass. Note different results obtained from different brightness temperatures used to define the cloud area. Dashed lines show the range of time-averaged eruption rates using the entire growth series, from Fig. 3.

min, as seen in Fig. 6b after ~17:00 UTC. This is a curious observation. Why would the lightning decrease once the MER stabilized at a constant, high rate? It appears that electrification was controlled by the rate of increase in MER, rather than the MER itself. Vent overpressure may have played a role here, as suggested by recent laboratory studies of volcanic lightning by Méndez Harper et al. (2018). The vigorous first ~50 min of plume development may have experienced more overpressured vent conditions, accelerating the flux of particles and promoting electrification. Alternatively, there may have been other (unknown) processes in this early stage from 16:10–17:00 UTC that enhanced electrification of the ash cloud, such as a shift in magma fragmentation, ash production, or external water involvement. Although nothing is immediately obvious from the field stratigraphy (Maeno et al., 2019), this would be an interesting avenue for future work.

For now, our existing observations may be summarized in this way: low-energy lightning during the first 50 min occurred during the vigorous increase in MER, suggesting (a) possible overpressured conditions at vent, and (b) well-mixed particles within the turbulent plume, favoring abundant small discharges rather than isolated large ones. Later, once the eruption rate held constant, there were fewer, higher-energy strokes, pointing to (a) reduction in vent overpressure, and (b) large-scale stratification within the ash cloud, creating isolated layers of charge and more powerful lightning.

After ~17:45 UTC, Kelud's eruption column became less stable, shedding ground-hugging currents visible in photographs (see Fig. 4d–f).

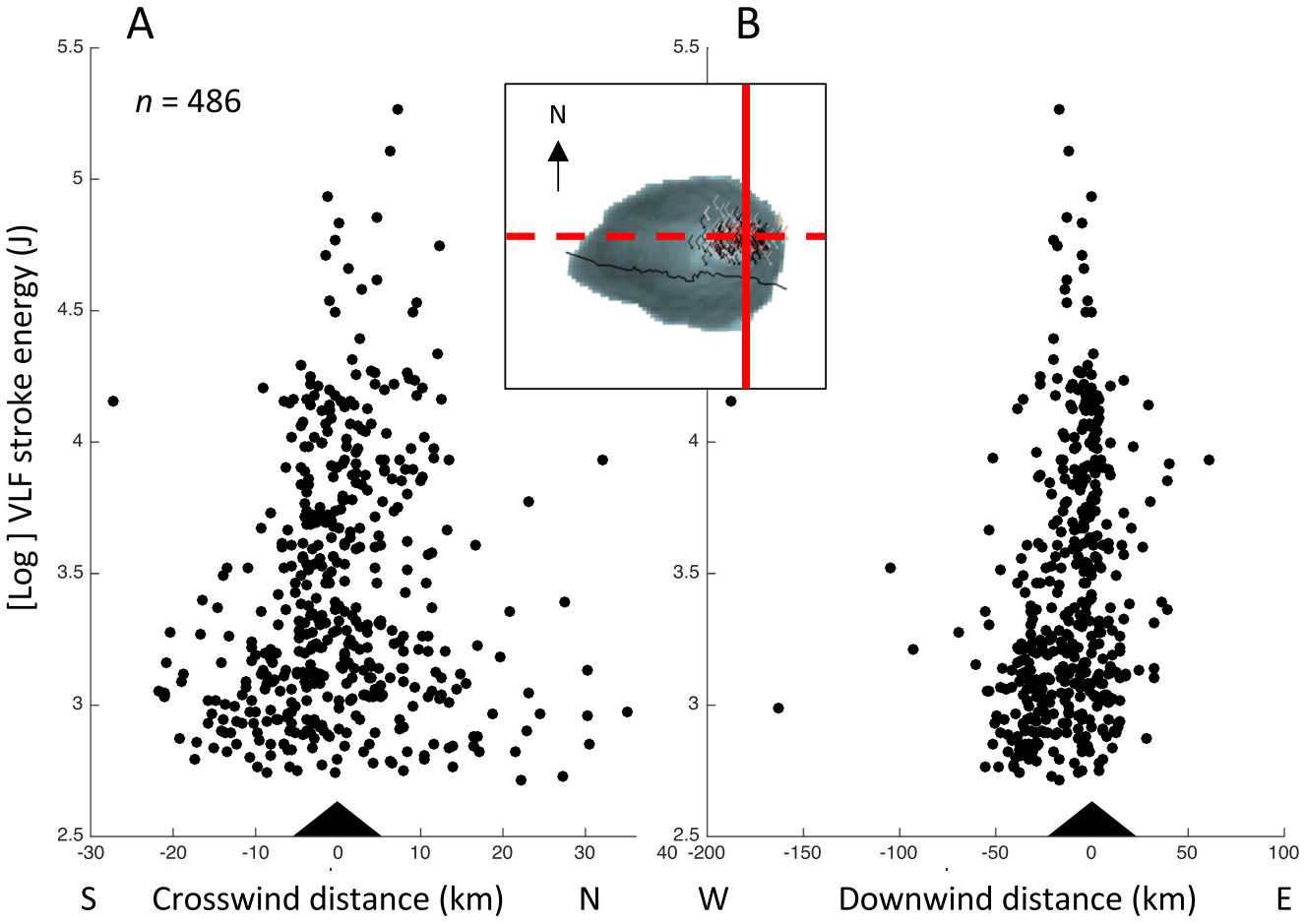

Fig. 7. Energy of volcanic lightning with respect to distance from Kelud volcano. VLF stroke energy in the 7–18 kHz band shown on a log10 scale. Each point represents one lightning stroke detected by WWLLN. (A) Strokes in the north-south, crosswind direction, and (B) east-west, downwind direction. Inset shows where these cross sections intersect the umbrella cloud at 17:50 UTC (from Fig. 3). Note roughly symmetrical distribution of stroke energies in the crosswind direction.

Lightning is surprisingly unresponsive to these changes. Stroke rates remain relatively low (≤2 per min), without any major shifts in stroke energy (Fig. 6a). This stands in contrast to the 2015 eruption of Calbuco volcano in Chile, which exhibited a spike in lightning activity during production of ground-hugging currents (Van Eaton et al., 2016). Both eruptions produced density currents of similar volume, and similar proportion of the overall erupted products (roughly 2–10% by volume; Castruccio et al., 2016; Maeno et al., 2019). These findings suggest that the highest stroke rates during an eruption may not always indicate a shift from buoyant to collapsing column, as was seen at Calbuco (Van Eaton et al., 2016). However, in both cases, the abrupt increase in lightning rates did signal an important change in eruption behavior. At Kelud it accompanied rapid intensification of the MER, and at Calbuco, the formation of pyroclastic density currents. The general suggestion here is that there may not be one lightning pattern that is universally diagnostic of an eruption process. Rather, transitions in eruption style, fragmentation processes, and water content appear to generate lightning in subtle and complex ways. Another key shared feature of the Kelud and Calbuco eruptions is that in both cases, the umbrella slowed its expansion rate after the column began shedding ground-hugging density currents (notice the decrease in apparent MER after 17:45 in Fig. 6b), which is a valuable process to recognize during eruption monitoring (Van Eaton et al., 2016).

4.3. 'Regular' vs. volcanic lightning

A separate, but related, question is how to distinguish volcanic lightning from standard thunderstorms. At present, there is no robust method for telling the two apart—when convective clouds develop over volcanoes, they commonly (a) trigger volcanic lightning alerts and (b) obscure satellite views of the vent. This is an almost daily occurrence in the tropics, particularly Indonesia and Papua New Guinea. Fig. 8 provides a glimpse into how we may address this issue in the future. The plot shows two weeks of lightning within 300 km of Kelud before and after the 2014 eruption, detected by the same network. The stroke energy of volcanic lightning is slightly higher than that of background thunderstorms, with fewer low-energy discharges ($<1 \times 10^3$ J). Although it would be valuable to consider seasonal changes and weather conditions unique to each volcanic environment, this first cut suggests that it may be possible to distinguish volcanic from non-volcanic lightning by leveraging (a) the decay of stroke-rate or stroke energy with distance from vent, as seen in Fig. 7, or (b) the statistical differences in stroke energy compared to background lightning, as seen in Fig. 8.

5. Conclusions

We have analyzed the WWLLN-detected volcanic lightning, umbrella-cloud expansion rates from satellite, and ground-based photographs to examine eruption processes during the 2014 eruption of Kelud volcano, Indonesia. Our main findings can be summarized by the following:

1. Rates of umbrella expansion indicate time-averaged mass eruption rates (MER) in the range of 8×10^7–1×10^8 kg s, with an uncertainty of +/− 50%. This is consistent with estimates from field mapping

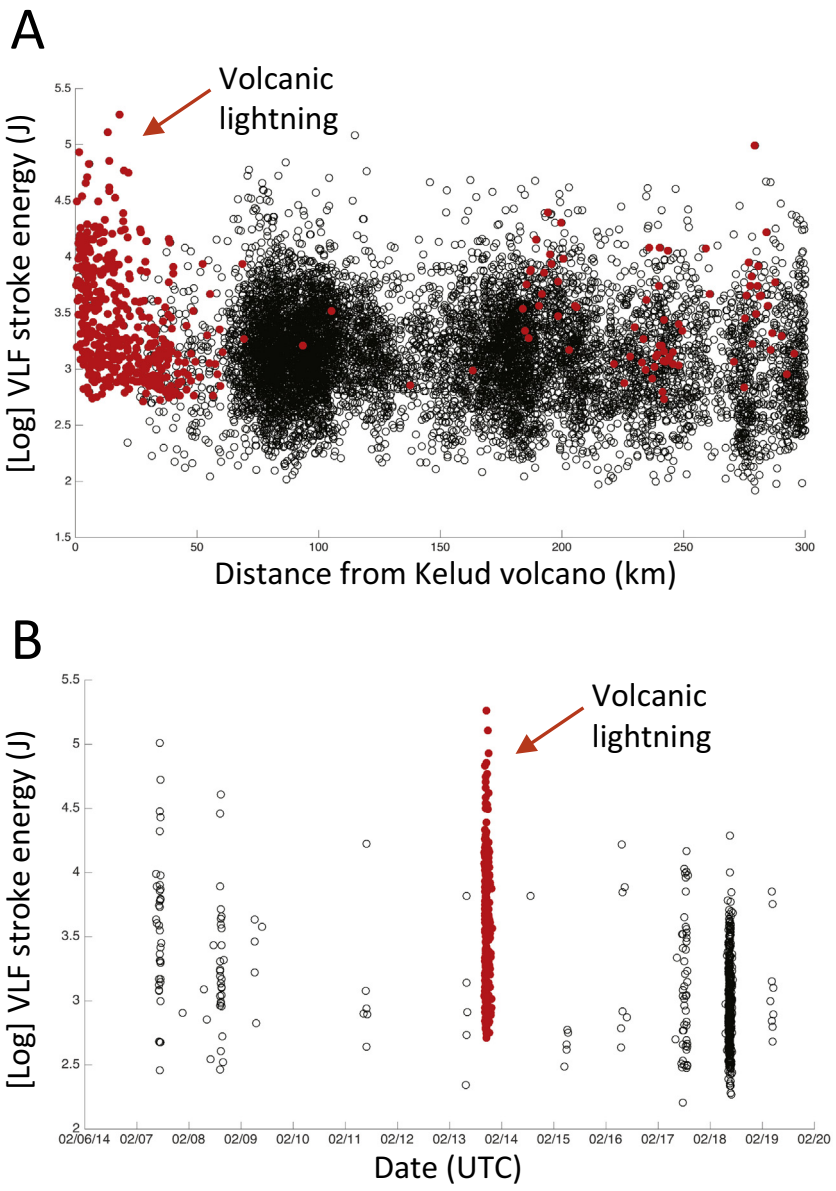

Fig. 8. Comparison of lightning VLF stroke energy from volcanic and non-volcanic lightning detected by WWLLN. Lightning associated with the Kelud eruption is shown in red. (A) Stroke energy vs. distance from Kelud, within 300 km of the volcano and within 3 days of 13 Feb 2014. Notice the absence of low-energy strokes ($<10^{2.5}$ J) in the volcanic lightning relative to background. (B) Stroke energy vs. time within a week of the eruption (n = 8835 strokes). Detections are constrained within a bounding box from 50 km west, 250 km east, and 100 km north and south of Kelud. Vertical axes use a log10 scale.

($3.7–9.3 \times 10^7$ kg s^{-1}: Maeno et al., 2019) and 3D numerical simulations (3×10^7–1×10^8 kg s^{-1}: Suzuki and Iguchi, 2019).

2. Incremental expansion rates calculated between each satellite pass show three stages of the climactic plinian eruption: (1) rapid intensification of the MER during the first hour (16:10–17:00 UTC), (2) stable MER for about an hour, and (3) waning toward the end (after ~17:50 UTC). During the waning stage, decreased flux into the umbrella cloud coincides with column instability and formation of pyroclastic density currents seen in photographs around 17:45 UTC.
3. We infer that some of the erupted mass partitioned into ground-hugging currents, leading to a slower expansion of the umbrella cloud and, therefore, lower apparent MER.
4. Overall lightning stroke-rates and energies are greatest within 50 km of the vent, even when the ash cloud extends >200 km downwind. This suggests lightning was focused in the regions of highest particle concentration and turbulence.
5. Lightning does not show a simple, direct correlation with MER over the course of eruption. We find that stroke rates increase sharply within the first 30–40 min of the climactic eruption (during rapid intensification), and drop below 2 per min once the MER stabilizes. The results point to lightning enhancement by accelerating particles, perhaps related to shock waves from an overpressured vent (Méndez Harper et al., 2018).
6. During this same time period, the eruption also generated fewer high-energy strokes, suggesting that the well-mixed, turbulent plume carried smaller 'pockets' of charge that favored lower-energy lightning (Behnke and Bruning, 2015).
7. A key finding is that abrupt shifts in lightning stroke-rates (which may be detectable in near-real time) reveal important changes in eruptive behavior and hazards.

Supplementary data to this article can be found online at https://doi.org/10.1016/j.jvolgeores.2018.10.016.

Acknowledgements

Kirstin Hargie acknowledges an undergraduate volunteer opportunity at the Cascades Volcano Observatory, and Alexa Van Eaton acknowledges a U.S. Geological Survey Mendenhall Fellowship. We thank Helen Webster, Supriyati Andreastuti, Heather Wright, Christina Widiwijayanti, Sonja Behnke, David Schneider, and Roger Denlinger for valuable discussions. The authors gratefully acknowledge Heppy Trishna Putra for providing the photographs used in this paper, and Jay Wellik for facilitating contact. We also wish to thank the World Wide Lightning Location Network (http://wwlln.net), a collaboration among over 50 universities and institutions, for providing the lightning location data. This project took advantage of netCDF software developed by UCAR/Unidata (http://doi.org/10.5065/D6H70CW6). The views, opinions, and findings contained in this report are those of the authors and should not be construed as an official National Oceanic and Atmospheric Administration or U.S. Government position, policy, or decision. Andrew Tupper, Fukashi Maeno, and Yujiro Suzuki provided constructive reviews that improved the manuscript.

References

Andreastuti, S., (2014). Kelud deposit stratigraphy (unpublished raw data).

Behnke, S.A., Bruning, E.C., 2015. Changes to the turbulent kinematics of a volcanic plume inferred from lightning data. Geophys. Res. Lett. 42, 4232–4239. https://doi.org/10.1002/2015gl064199.

Behnke, S.A., Thomas, R.J., McNutt, S.R., Schneider, D.J., Krehbiel, P.R., Rison, W., Edens, H.E., 2013. Observations of volcanic lightning during the 2009 eruption of Redoubt Volcano. J. Volcanol. Geotherm. Res. 259, 214–234. https://doi.org/10.1016/j.jvolgeores.2011.12.010.

Behnke, S.A., Edens, H.E., Thomas, R.J., Smith, C.M., McNutt, S.R., Van Eaton, A.R., Cimarelli, C., Cigala, V., 2018. Investigating the origin of continual radio frequency impulses during explosive volcanic eruptions. J. Geophys. Res. Atmos. 123 (8), 4157–4174. https://doi.org/10.1002/2017jd027990.

Carey, S., Sparks, R.S.J., 1986. Quantitative models of the fallout and dispersal of tephra from volcanic eruption columns. Bull. Volcanol. 48 (2–3), 109–125. https://doi.org/10.1007/BF01046546.

Castruccio, A., Clavero, J., Segura, A., Samaniego, P., Roche, O., Le Pennec, J.-L., Droguett, B., 2016. Eruptive parameters and dynamics of the April 2015 sub-Plinian eruptions of Calbuco volcano (southern Chile). Bull. Volcanol. 78 (9). https://doi.org/10.1007/s00445-016-1058-8.

Caudron, C., Taisne, B., Garcés, M., Alexis, L.P., Mialle, P., 2015. On the use of remote infrasound and seismic stations to constrain the eruptive sequence and intensity for the 2014 Kelud eruption. Geophys. Res. Lett. 42 (16), 6614–6621. https://doi.org/10.1002/2015gl064885.

Cimarelli, C., Alatorre-Ibargüengoitia, M.A., Kueppers, U., Scheu, B., Dingwell, D.B., 2014. Experimental generation of volcanic lightning. Geology 42 (1), 79–82. https://doi.org/10.1130/G34802.1.

Costa, A., Folch, A., Macedonio, G., 2013. Density-driven transport in the umbrella region of volcanic clouds: implications for tephra dispersion models. Geophys. Res. Lett. 40 (18), 4823–4827. https://doi.org/10.1002/grl.50942.

Deierling, W., Petersen, W.A., Latham, J., Ellis, S., Christian, H.J., 2008. The relationship between lightning activity and ice fluxes in thunderstorms. J. Geophys. Res. 113, D15210. https://doi.org/10.1029/2007jd009700.

Ewert, J.W., Holzworth, R.H., Diefenbach, A.K., 2010. Global Detection of Explosive Volcanic Eruptions With the World Wide Lightning Location Network (WWLLN) and Application to Aviation Safety. Abstract AE31A-04 Presented at 2010 Fall Meeting, AGU, San Francisco, California, 13–17 December.

Fee, D., Haney, M.M., Matoza, R.S., Van Eaton, A.R., Cervelli, P., Schneider, D.J., Iezzi, A.M., 2017. Volcanic tremor and plume height hysteresis from Pavlof Volcano, Alaska. Science 355, 45–48.

Haney, M.M., Van Eaton, A.R., Lyons, J.J., Kramer, R.L., Fee, D., Iezzi, A.M., 2018. Volcanic thunder from explosive eruptions at Bogoslof volcano, Alaska. Geophys. Res. Lett. 45. https://doi.org/10.1002/2017GL076911.

Hoblitt, R.P., 2000. Was the 18 May 1980 lateral blast at Mt St Helens the product of two explosions? Phil. Trans. R. Soc. London A358, 1639–1661. https://doi.org/10.1098/rsta.2000.0608.

Hutchins, M.L., Holzworth, R.H., Brundell, J.B., Rodger, C.J., 2012a. Relative detection efficiency of the World Wide Lightning Location Network. Radio Sci. 47 (6), RS6005. https://doi.org/10.1029/2012rs005049.

Hutchins, M.L., Holzworth, R.H., Rodger, C.J., Heckman, S., Brundell, J.B., 2012b. WWLLN absolute detection efficiencies and the global lightning source function. Geophys. Res. Abstr. 14, EGU2012–12917.

Iwasaki, H., 2015. Climatology of global lightning classified by stroke energy using WWLLN data. Int. J. Climatol. 35 (14), 4337–4347. https://doi.org/10.1002/joc.4291.

Kanamori, H., Mori, J., 1992. Harmonic excitation of mantle Rayleigh waves by the 1991 eruption of Mount Pinatubo, Philippines. Geophys. Res. Lett. 19 (7), 721–724.

Kristiansen, N.I., Prata, A.J., Stohl, A., Carn, S.A., 2015. Stratospheric volcanic ash emissions from the 13 February 2014 Kelut eruption. Geophys. Res. Lett. 42, 588–596. https://doi.org/10.1002/2014gl062307.

Lechner, P., Tupper, A., Guffanti, M., Loughlin, S., Casadevall, T., 2017. Volcanic ash and aviation—the challenges of real-time, global communication of a natural hazard. Adv. Volcanol. https://doi.org/10.1007/11157_2016_49.

Lyons, J.J., Haney, M.M., Van Eaton, A.R., Schwaiger, H.F., Schneider, D.J., 2013. Seismoacoustic Analysis of Ultra-Long-Period Signals Generated in the Atmosphere during the 2009 Eruption of Redoubt Volcano, Alaska. Abstract S23B-2496 Presented at 2013 Fall Meeting, AGU, San Francisco, Calif., 9–13 Dec.

Maeno, F., Nakada, S., Yoshimoto, M., Shimano, T., Hokanishi, N., Zaennudin, A., Iguchi, M., 2019. A sequence of a plinian eruption preceded by dome destruction at Kelud volcano, Indonesia, on February 13, 2014, revealed from tephra fallout and pyroclastic density current deposits. J. Volcanol. Geotherm. Res. 382, 24–41.

Mastin, L.G., 2014. Testing the accuracy of a 1-D volcanic plume model in estimating mass eruption rate. J. Geophys. Res. 119, 2474–2495. https://doi.org/10.1002/2013JD020604.

Mastin, L.G., Van Eaton, A.R., Lowenstern, J.B., 2014. Modeling ash fall distribution from a Yellowstone supereruption. Geochem. Geophys. Geosyst. 15, 3459–3475. https://doi.org/10.1002/2014GC005469.

Méndez Harper, J.S., Dufek, J., 2016. The effects of dynamics on the triboelectrification of volcanic ash. J. Geophys. Res. Atmos. 121 (14), 8209–8228. https://doi.org/10.1002/2015jd024275.

Méndez Harper, J.S., Cimarelli, C., Dufek, J., Gaudin, D., Thomas, R.J., 2018. Inferring compressible fluid dynamics from vent discharges during volcanic eruptions. Geophys. Res. Lett. https://doi.org/10.1029/2018gl078286.

Morton, B.R., Taylor, G.I., Turner, J.S., 1956. Turbulent gravitational convection from maintained and instantaneous sources. Proc. R. Soc. London, Ser. A, A234 https://doi.org/10.1098/rspa.1956.0011.

Nakashima, Y., Heki, K., Takeo, A., Cahyadi, M.N., Aditiya, A., Yoshizawa, K., 2016. Atmospheric resonant oscillations by the 2014 eruption of the Kelud volcano, Indonesia, observed with the ionospheric total electron contents and seismic signals. Earth Planet. Sci. Lett. 434, 112–116. https://doi.org/10.1016/j.epsl.2015.11.029.

Pouget, S., Bursik, M., Webley, P., Dehn, J., Pavolonis, M., 2013. Estimation of eruption source parameters from umbrella cloud or downwind plume growth rate. J. Volcanol. Geotherm. Res. 258, 100–112. https://doi.org/10.1016/j.jvolgeores.2013.04.002.

Pouget, S., Bursik, M., Johnson, C.G., Hogg, A.J., Phillips, J.C., Sparks, R.S.J., 2016. Interpretation of umbrella cloud growth and morphology: implications for flow regimes of short-lived and long-lived eruptions. Bull. Volcanol. 78 (1). https://doi.org/10.1007/s00445-015-0993-0.

Ripepe, M., De Angelis, S., Lacanna, G., Voight, B., 2010. Observation of infrasonic and gravity waves at Soufrière Hills Volcano, Montserrat. Geophys. Res. Lett. 37 (19), L00E14. https://doi.org/10.1029/2010gl042557.

Ripepe, M., Barfucci, G., De Angelis, S., Delle Donne, D., Lacanna, G., Marchetti, E., 2016. Modeling Volcanic Eruption Parameters by Near-Source Internal Gravity Waves. Sci. Rep. 6, 36727. https://doi.org/10.1038/srep36727.

Smith, C.M., Van Eaton, A.R., Charbonnier, S., McNutt, S.R., Behnke, S.A., Thomas, R.J., Edens, H.E., Thompson, G., 2018. Correlating the electrification of volcanic plumes with ashfall textures at Sakurajima Volcano, Japan. Earth Planet. Sci. Lett. 492, 47–58. https://doi.org/10.1016/j.epsl.2018.03.052.

Sparks, R.S.J., 1986. The dimensions and dynamics of volcanic eruption columns. Bull. Volcanol. 48, 3–15. https://doi.org/10.1007/BF01073509.

Suzuki, Y.J., Iguchi, M., 2019. Determination of the mass eruption rate for the 2014 Mount Kelud eruption using three-dimensional numerical simulations of volcanic plumes. J. Volcanol. Geotherm. Res. 382, 42–49.

Suzuki, Y.J., Koyaguchi, T., 2009. A three-dimensional numerical simulation of spreading umbrella clouds. J. Geophys. Res. 114, B03209. https://doi.org/10.1029/2007jb005369.

Suzuki, Y.J., Costa, A., Cerminara, M., Esposti Ongaro, T., Herzog, M., Van Eaton, A.R., Denby, L.C., 2016. Inter-comparison of three-dimensional models of volcanic plumes. J. Volcanol. Geotherm. Res. 326, 26–42. https://doi.org/10.1016/j.jvolgeores.2016.06.011.

Van Eaton, A.R., Mastin, L.G., Herzog, M., Schwaiger, H.F., Schneider, D.J., Wallace, K.L., Clarke, A.B., 2015. Hail formation triggers rapid ash aggregation in volcanic plumes. Nat. Commun. 6, 7860. https://doi.org/10.1038/ncomms8860.

Van Eaton, A.R., Amigo, Á., Bertin, D., Mastin, L.G., Giacosa, R.E., González, J., Valderrama, O., Fontijn, K., Behnke, S.A., 2016. Volcanic lightning and plume behavior reveal evolving hazards during the April 2015 eruption of Calbuco volcano, Chile. Geophys. Res. Lett. https://doi.org/10.1002/2016GL068076.

Webster, H.N., Devenish, B.J., Mastin, L.G., Thomson, D.J., Van Eaton, A.R., 2018. Operational modelling of umbrella cloud growth in a lagrangian volcanic ash transport and dispersion model (in preparation).

Woods, A.W., Kienle, J., 1994. The dynamics and thermodynamics of volcanic clouds; theory and observations from the April 15 and April 21, 1990 eruptions of Redoubt Volcano, Alaska. J. Volcanol. Geotherm. Res. 62 (1–4), 273–299.